Numerical Modelling of HTPEM Fuel Cell

Vamsi Ambala

A Thesis Submitted to

Indian Institute of Technology Hyderabad

In Partial Fulfillment of the Requirements for
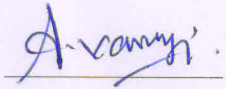
The Degree of Master of Technology

भारतीय प्रौद्योगिकी संस्थान हैदराबाद
Indian Institute of Technology Hyderabad

Department of Chemical Engineering

June 2019

Declaration

I declare that this written submission represents my ideas in my own words, and where ideas or words of others have been included, I have adequately cited and referenced the original sources. I also declare that I have adhered to all principles of academic honesty and integrity and have not misrepresented or fabricated or falsified any idea/data/fact/source in my submission. I understand that any violation of the above will be a cause for disciplinary action by the Institute and can also evoke penal action from the sources that have thus not been properly cited, or from whom proper permission has not been taken when needed.
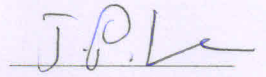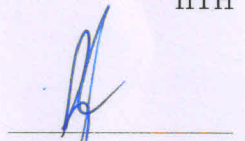
(Vamsi Ambala)

CH17MTECH11003
(Roll No.)

Approval Sheet

This Thesis entitled "Numerical Modelling of HTPEM Fuel Cell" by Vamsi Ambala is approved for the degree of Master of Technology from IIT Hyderabad

(Dr. Phanindra Jampana) Examiner
Dept. of Chem Eng
IITH

(Dr. Parag D Pawar) Examiner
Dept. Chem Eng
IITH

(Dr. Vinod M Janardhanan) Adviser
Dept. of Chem Eng
IITH

(Dr. Raja Benerjee) Chairman
External Examiner
Dept. of Mech Eng
IITH

Acknowledgements

Dedication

To my forever loving family and friends

Abstract

As we are seeing today, world is in a crisis of air pollution due to inevitable usage of fossil fuels in automobiles to run. The pollution is mainly due to emission of toxic gases such as carbon monoxide and oxides of nitrogen. There is a immense need of creating an alternate source of energy which reduces the level of emissions. **Fuel cell** is a device that can produce electricity without the generation of any pollutants when operated on pure H_2 fuel. Low temperature polymer electrolyte membrane fuel cells operate at around 80 °C and water management in these cells becomes a challenge. This problem can be cirumvented if the cell can be operated above 100 °C. High temperature polymer electrolytic membrane fuel cells operate in the range of 120 °C to 200 °C with phosphoric acid doped polybenzimidazole as membrane electrolyte [4]. Modelling helps in understanding the deep insight of fuel cell processes thereby facilitates the improvement without involving any experimental work. In our work 1-D model is formed and resolved along the thickness of MEA. Validation of model is done for [1],[3] and [10] by generating polarization curves, cathode and anode overpotentials, and CO dynamic response.

CONTENTS

CHAPTER 1

INTRODUCTION

Due to increase in global warming which is caused by green house gas emission which in turn resulted by the use of fossil fuel products such as petrol, diesel etc. There is a huge responsibility on us to bring down these emissions and protect our earth. In addition combustion of fossil fuels also leads to the emission of carbon monoxide (CO), carbondioxide (CO_2) and oxides of nitrogen (NO_X). Even though we know emissions from fossil fuel are detrimental to our nature and fossil fuel reserves are dwindling day by day we can not avoid using them because of their versatile demand. So there is a necessity to look for an alternative source which gives the clean and green energy. But can we do produce energy with zero emission of noxious gases ? Yes we can. We can produce clean and green energy with **Fuel Cell** which utilizes mainly Hydrogen (H_2) and Oxygen (O_2).

First fuel cell was invented in 1839 by Sir William Grove in which he first carried out electrolysis of dilute sulfuric acid, confined Hydrogen (H_2) and Oxygen (O_2) in two separate glass tubes. He connected an ammeter to the glass tubes in which a small electric current signal was detected arised from the oxidation of Hydrogen (H_2) and reduction of Oxygen (O_2) on individual Pt electrodes. Eventhough fuel cells do produce clean energy their power density is small. So multiple fuel cells are connected in series called **fuel cell stacks** to produce the required power.

1.1 Fuel Cell Fundamentals

A Fuel cell is an electrochemical conversion device which converts chemical energy of a substance to electrical energy. It takes Hydrogen (H_2) as fuel, Oxygen (O_2) as oxidant and produces electricity. Water (H_2O) formation and heat liberation take place as a part of the process.

1.1.1 Construction

Fuel cell comprises mainly of three components (Fig. 1.1) namely
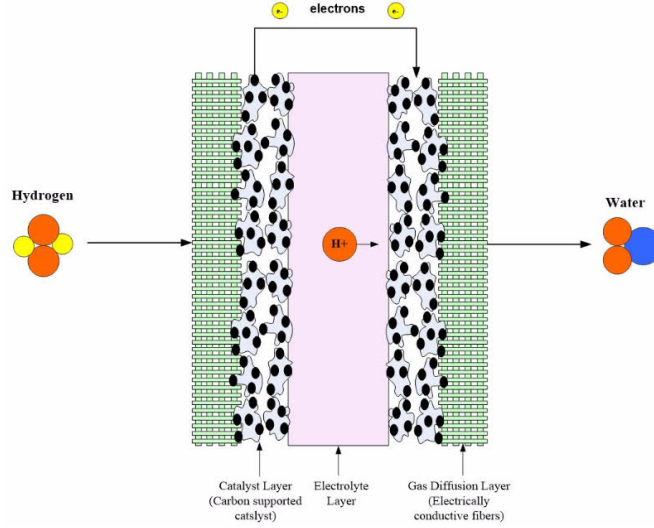
1. Anode

2. Cathode

3. Electrolyte

Figure 1.1: Schematic representation of a fuel cell

Anode and cathode are called electrodes and each electrode contains two layers

- Gas diffusion layer (GDL)

    - Immediate to the fuel channel and gives support to the catalyst layer.

- Catalyst/Reaction layer (CL)

    - After reactant is passed through the GDL it reaches CL and reacts here.

The structure of electrodes and electrolyte all together is called Membrane Electrode Assembly (MEA) which is shown in Fig. 1.1.

Apart from it, auxilary parts like bipolar plates through which fuel and oxidant are sent, end plates and gaskets (to cut the leakage of reactant gases) are incorporated in fuel cell as shown in Fig. 1.2.

1.1.2 Principle

Fuel cell takes Hydrogen (H_2) on anode side and Oxygen (O_2) on cathode side. The main principle underlying in the operation of a fuel cell is half cell reactions namely Hydrogen Oxidation Reaction (HOR) which occurs at anode (Eq. 1.1) and Oxygen Reduction Reaction (ORR) which occurs at cathode (Eq. 1.2). Eq. 1.3 represents the overall reaction occuring inside a fuel cell.

$$H_2 \rightleftharpoons 2H^+ + 2e^- \tag{1.1}$$

$$\frac{1}{2}O_2 + 2H^+ + 2e^- \rightleftharpoons H_2O \tag{1.2}$$

$$H_2 + \frac{1}{2}O_2 \rightleftharpoons H_2O + \text{electricity} \tag{1.3}$$
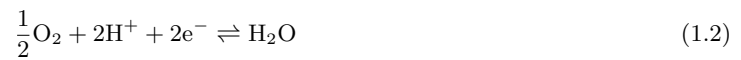
As we are sending H_2 through fuel side channel (anode side) it diffuses through the anode GDL and reaches anode CL where Hydrogen Oxidation Reaction(Eq. 1.1) takes place resulting in release of protons and electrons. Similarly O_2 is send on cathode side which reaches cathode CL after diffusion through the cathode
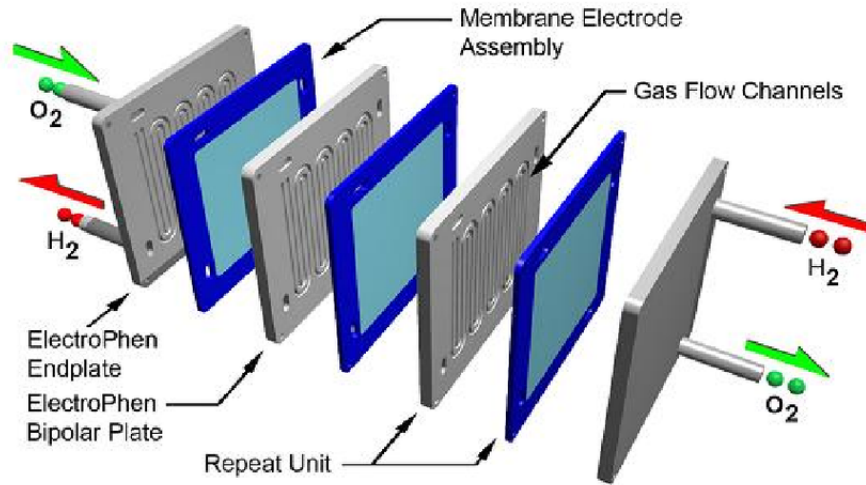
Figure 1.2: Schematic of fuel cell assembly

GDL. The difference between ionic and electronic charges on both sides causes charges to transfer from the anode side to cathode side. Protons (H^+) pass through the electrolyte which does not allow electrons (e^-) to pass through it. To facilitate the flow of electrons towards the cathode side an external load is connected between anode and cathode catalyst layers producing electronic current. After successful passage of ions they combine with O_2 according to Eq. 1.2 on the CL of cathode completing the overall reaction (Eq. 1.3) resulting in production of water.

1.1.3   Types of Fuel Cell

The process that is occuring inside the fuel cell is electrons must pass through the external load provided and protons through the electrolyte. Fuel cell is differentiated by their type of electrolyte, their mechanism of reaction and operating temperature range change according to it.

The five types of fuel cell are:

1. Polymer electrolytic membrane fuel cell (PEMFC)

2. Phosphoric acid fuel cell (PAFC)

3. Alkaline fuel cell (AFC)

4. Molten carbonate fuel cell (MCFC)

5. Solid oxide fuel cell (SOFC)

Table 1.1 provide details of fuel cells with operating temperature range, type of electrolyte used, charge carrier, catalyst prefered on electrodes etc.

Among these PEMFC and SOFC are used commercially.

3

Table 1.1: Table showing different types of fuel cells

Name	Electrolyte	Charge carrier	Temperature	Catalyst	Cell components	Fuel
PEMFC	Polymer membrane	H^+	$80 - 160\,^\circ C$	Platinum	Carbon based	H_2, methanol
PAFC	Liquid H_3PO_4	H^+	$200\,^\circ C$	Platinum	Carbon based	H_2
AFC	Liquid KOH	OH^-	$60 - 220\,^\circ C$	Platinum	Carbon based	H_2
MCFC	Molten carbonate	CO_3^{2-}	$650\,^\circ C$	Nickel	SS based	H_2, CH_4
SOFC	Ceramic	O^{2-}	$600 - 1000\,^\circ C$	Perovskites	Ceramic based	H_2,CH_4,CO

PEMFCs employ a thin membrane made with polymer and based on their operating temperature range they are further divided into

- Low temperature PEMFC and

- High temperature PEMFC

Low temperature PEM fuel cells are generally operated below 80 °C and employ a thin Nafion based membrane. Major drawbacks of LTPEM are water management and no tolerance for impurities. Whereas HTPEM fuel cells operate in the range of 120-160 °C and employ phosphoric acid doped polybenzimidazole (PBI) as a membrane electrolyte. Drawbacks of LTPEM can be overcome by operating the cell at increased temperatures. Advantages of HTPEM are increased performance through increased reaction kinetics and CO tolerance which comes mainly with H_2.

Mechanism: PEM follows the same mechanism given in Eq. 1.1 and Eq. 1.2

SOFCs employ a solid electrolyte made of ceramic. The most common electrolyte material used is yttria-stabilized zirconia (YSZ) which is an oxygen vacant ionic conductor. As mentioned in table 1.1 charge carrier is O^{2-} and the mechanism is

$$H_2 + O^{2-} \rightarrow H_2O + 2e^- \tag{1.4}$$

$$\frac{1}{2}O_2 + 2e^- \rightarrow O^{2-} \tag{1.5}$$

In PEMFC water is produced on the cathode side whereas in SOFC it is produced on anode side as given by Eq. 1.4.

1.2 Recent Developments

In the city of Delhi the capital of India mankind is undergoing hardship due to exessive air pollution. Even the government has incepted odd and even rule for vehicles. The Supreme Court has directed the government of Delhi to explore the feasibility of hydrogen-powered buses for its public transport fleet. The Delhi government had notified the court that it had initiated the process of procuring 1000 electric buses. The court said that it would be better to switch from CNG to hydrogen fuel instead and highlighted the fact that hydrogen buses have been successfully introduced in various countries including in the state of California in the US. In India, Tata Motors has started manufacturing hydrogen-powered buses as well. It is said that Hydrogen-powered buses have a range of 400 km and are claimed to have lower running costs compared to conventional buses.

A team of engineers at Washington Unversity in St. Louis has developed a high power fuel cell using a pH enabled microscale bipolar interface (PMBI). It could power a variety of transportation modes including unmanned underwater vehicles, drones and electric aircraft with lower cost. This fuel cell is modified using a acidic electrolyte at one eletrode and a alkaline electrolyte at the other electrode. Both electrolytes are separated using PMBI. A sharp pH gradient is formed between two electrolytes which enables the operation of the system.

According to a report by OFweek Industry Research Center China manufactured 1,619 hydrogen fuel-cell vehicles in 2018, which is up 27% from 2017.The company Zhongtong Bus was ranked the top manufacturer of fuel cell vehicles in 2018 with a total of 790 fuel cell vehicles produced. On December 29, 2018, 20 fuel cell buses made by Yutong hit the road, marking a new upgrade of the public transport system in Henan province. Compared with electric city buses, the fuel cell city buses boast short hydrogen refueling time and longer driving range. Based on the current specification of the vehicle, it takes 10 minutes to fully refueling the hydrogen, and has a driving range of about 500 km. It is also reported that Yutong will continue to develop fuel cell vehicles, make breakthrough in terms of core technologies including fuel cell vehicles, fuel cell system and hydrogen system, establish a completed test evaluation system of fuel cells, and achieve the industrialized promotion of fuel cell buses.

CHAPTER 2

CHARACTERIZATION TECHNIQUES

2.1 Performance of a Fuel Cell

HTPEM fuel cell takes hydrogen and oxygen in order to produce electricity. Since hydrogen has limited sources it must be utilized as much as possible with in a fuel cell. It is customary to use air in place of oxygen but the ORR on cathode side is very sluggish due to the presence of other gases. For a fuel cell efficiency is of great importance. As thermodynamics tells electric work obtainable from fuel cell is limited by the Gibbs free energy of the reacion specified which in turn decides the efficiency(η). The maximum voltage obtainable from a fuel cell is determined by the its thermodynanmics and given by Nersnt equation.

$$E = E^0 - \frac{RT}{nF} ln \frac{\pi a_{products}^{v_i}}{\pi a_{reactants}^{v_i}} \tag{2.1}$$

Where E^0 is standard thermodynamic voltage and is given by

$$E^0 = \frac{\Delta g^0}{nF} \tag{2.2}$$

Where, Δg^0 = Standard Gibbs free energy of the reaction(J).

n = number of moles of electrons(mol).

F = Faraday constant(C/mol).

T = Temperature(K).

R = Gas constant(J/mol.K).

v_i = stoichiometric coefficient.

a_i = activity of ith component, since water is in liquid state activity is taken as unity, for hydrogen and oxygen activity is expressed in terms of partial pressures(p_{H_2} and p_{O_2}).

Efficiency of a fuel cell is given as the ratio of operating voltage(V) to the thermodynamically obtainable voltage(E).

$$\eta = \frac{\text{Operating voltage(V)}}{\text{Thermodynamic voltage(E)}} \tag{2.3}$$

So to accomplish maximum utilization of fuel we need to identify the losses that are decreasing the efficiency.

6

2.1.1 Various Losses in a Fuel Cell

To identify the sources of losses we have to analyse the process right from the reactant delievery to the product removal. There are mainly three types of losses. Those are

1. **Concentration losses**

   - These losses are attributed to the transport of reactant and oxidant from flow field plate to the catalyst layer through the porous gas diffusion layer.

   - These are mainly araised due to diffusional resistances.

   - At high current loads fuel consumption will be more so to avail the fuel for the reaction reactant transport must be fast enough.

2. **Activation losses**

   - These losses denote sluggishness in electrochemical reaction.

   - Faster the reaction more the electrons production.

   - To produce the more current density surface to volume ratio of the catalyst layer to be high so layer is made thin.

   - As compared to HOR on anode side ORR on cathode side is more sluggish due to the presence of other gases such as nitrogen.

3. **Ohmic losses**

   - These losses araise during transport of electrons and ions from anode to cathode.

   - Electrons do not experience resistance as long as external load is provided to facilitate the flow. But ions have to pass through the electrolyte which works on hopping mechanism causes delay in reaching the cathode side.

2.2 Various Techniques

To identify the losses we need to analyse the fuel cell and know what is happening inside. Characterization helps in understanding the performance and to distinguish good fuel cells from that of bad ones. Various parameters are obtained by charactarizing the fuel cell. Characterization techniques are mainly two types.

- Ex-situ Characterization Techniques

  - These are carried out for individual components of a fuel cell.

  - Fuel cell should be in unassembled form to characterize the structure and properties of components.

  - This type includes determination of porosity, surface area, structure and chemical composition.

- In-situ Characterization Techniques

  - These techniques interplay with voltage, current and time to characterize the fuel cell under operating conditions.

We will discuss In-situ techniques briefly

2.2.1 In-situ Techniques:

These techniques involve measurement of voltage and current which are the ultimate indicators of the performance and their measurement can be done in two ways.

- Potentiostatic

  - The voltage of fuel cell is set at particular value and corresponding current response is monitored.

  - It can be done either in steady state (where voltage does not vary with time) or dynamic state (where voltage vary with time).

- Galvanostatic

  - The current of a fuel cell is kept constant and voltage output is measured.

  - Galvanostatic also can be done in steady state (where voltage does not vary with time) and dynamic state (where voltage vary with time).

1. **Current-Voltage (iV) Measurement**
   iV measurement is the best technique to summarize the overall performance of a fuel cell and can be done potentiostatically or galvanostatically. In steady state mode both the methods will give same response for given voltage and current values. First voltage or current should be kept at a fixed value and respective current or voltage value should be taken down. This is repeated for a range of values required on iV plot that is made with i(A/cm^2) on X-axis and V(V) on Y-axis. During iV measurement fuel cell system should ensure steady state. After setting voltage it is needed to give fuel cell sometime to relax to reach steady state from dynamic state. The curves on the plot are called polarization (shifting of voltage from equillibrium value) curves.

   iV plot is shown in the fig 2.1. When no current is drawn from the fuel cell, voltage is ideal as given by the Eq. 2.1. As more current is drawn voltage drops due to irreversible losses as described above. The diffrence between operating voltage and theoratical voltage is named as overpotential. In low current density regions losses due to reaction kinetics are predominant (activation overpotential). As more current is drawn resistance offered to the flow of protons and electrons prevails (ohmic overpotential). At high current densities mass transport becomes slow hence concentraion losses will be more (concentration overpotential). This shows the overall view of voltage and current profiles.

2. **Cyclic Voltammetry**
   Cyclic volammetry is the most used technique in electrochemistry. It provides the information about catalyst activity. Information about thermodynamics and kinetics can be obtained by this technique. In this method voltage of the system is swept back and forth between two voltage limits and the resulting current response is measured. The plot of resulted current response and voltage swept is called cyclic voltammogram [Fig. 2.2]

3. **Current Interrupt Measurement**
   This technique is widely accepted in fuel cell research since it is very fast and can be conducted in parallel with iV measurement. It is mainly used for characterization of large fuel cells. The basic idea of this technique is when constant-current load is interrupted, it results in time dependent voltage response which is indication of resistive and capacitive behaviour of components of fuel cell. Resistors and capacitors are components of equivalent circuit models which we will discuss in following section. It provides information about reaction kinetics and mass transport processes.

4. **Electrochemical Impedance Spectroscopy**
   As given by ohms law resistance is the ratio of voltage to current is applied to direct current which is a
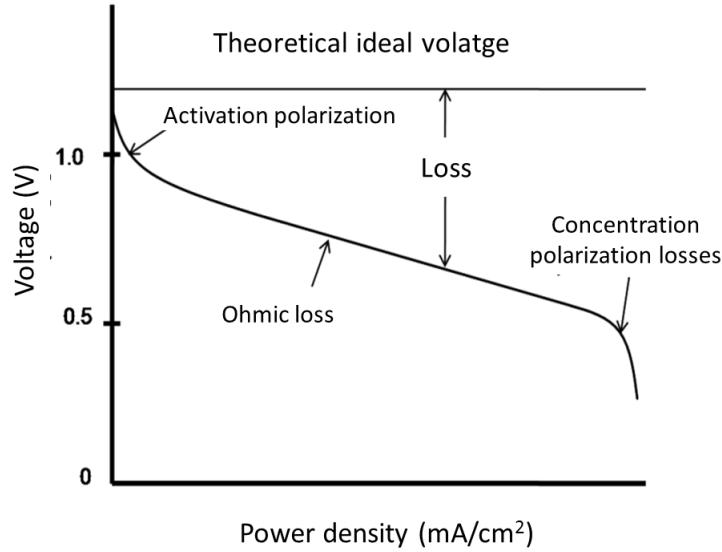
Figure 2.1: Interpretation of iV measurement

constant value (time independent). Polarization(iV) curves are obtained in this mode being invariant with time. iV curves do just summarizes the performance of fuel cell, EIS gives a deeper insight of processes occuring inside it. EIS is a dynamic technique which utilizes the alternating current to find the behaviour of fuel cell. Impedance is defined as the ratio of alternate voltage to alternate current and is denoted by Z.

$$Z = \frac{V(t)}{I(t)} \tag{2.4}$$

When fuel cell is running in steady state position, its sinusoidal voltage is perturbed with small amplitude V_o (in mV) and resulting current response is also sinusoidal with same period as voltage but with different amplitude I_o and with some phase shift ϕ as shown in Fig. 2.3. Choosing a small amplitude of perturbation is important to ensure linearity in the system. The voltage and current responses as a function of time are used to obtain impedance. Impedances is a complex number having resisance as real part and reactance as imaginary part. This perturbation is repeated for frequency range and a impedance plot is constructed by plotting real part on x-axis and imaginary part on y-axis. The plot constructed in this way is called Nyquist plot.

The losses occuring inside the fuel cell are identified by comparing them with the equivalent circuit models.

Equivalent Circuit Modelling

The main losses that are taking place inside the fuel cell are

(a) Activation losses.

(b) Ohmic losses

(c) Concentraion losses.

Activation losses on both anode and cathode side are assumed to be the result of resistance due to charge transfer and charge accumulation on the surface and are modelled using a **resistor**(R) and a
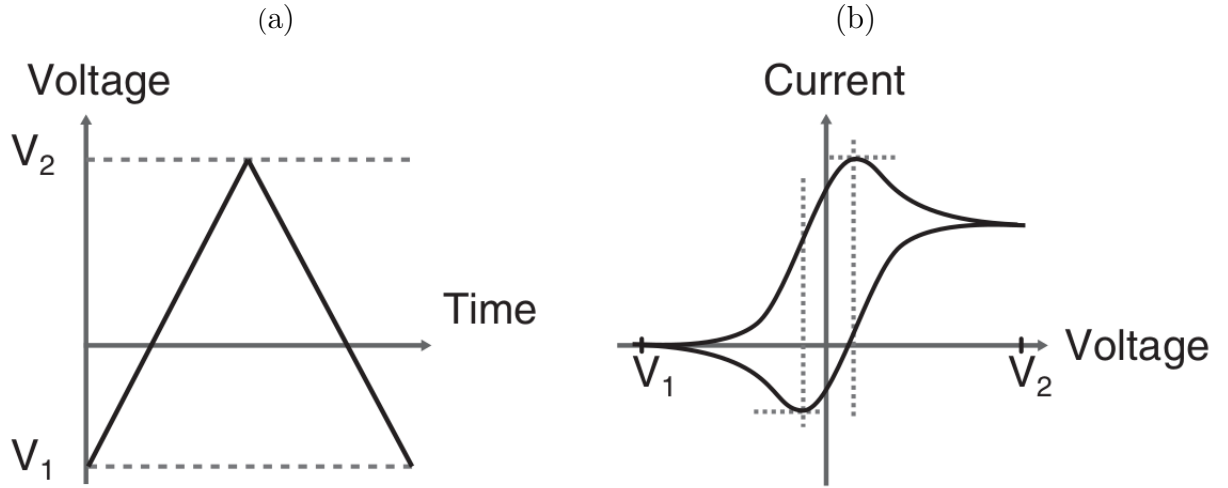
9

Figure 2.2: Representation of CV waveform. (a) Sweeping of voltage back and forth. (b) Current response as function of voltage swept

capacitor(C) respectively connected in parallel [11],[6].

$$Z_{\text{activation}} = \frac{R}{1 + j\omega CR} \tag{2.5}$$

Ohmic losses are modelling using a resistor since only resistance is residing in the electrolyte [11],[6].

$$Z_{\text{ohmic}} = R_{\text{electrolyte}} \tag{2.6}$$

Concentration or mass transport losses are modelled using warburg element [11],[6] and given by

$$Z_{\text{conc}} = \frac{\sigma_i}{\sqrt{\omega}}(1 - j) \tag{2.7}$$

Where σ_i is the warburg coefficient.

General EC model for a fuel cell is given by Randles circuit [7] which is the combination of two RC constants separated by a R as shown in Fig. 2.4 and Q is the constant phase element which shows up when capacitance is not assumed 100% and given as $C_{\text{dl}} = Q(j\omega)^{\alpha}$, where α is a CPE parameter.

Sinusoidal perturbation

The sinusoidal voltage perturbation introduced to the system is given by

$$V_{\text{cell}} = V_{\text{st}} + V_{\text{p}}\sin(\omega t) \tag{2.8}$$

Where, $V_{\text{cell}} =$ Voltage of the cell (V),
$V_{\text{st}} =$ Steady state voltage before perturbation(V),
$V_{\text{p}} =$ Perturbation amplitude (V),
$\omega =$ radian frequency (rad/s) and given as $\omega = 2\pi f$
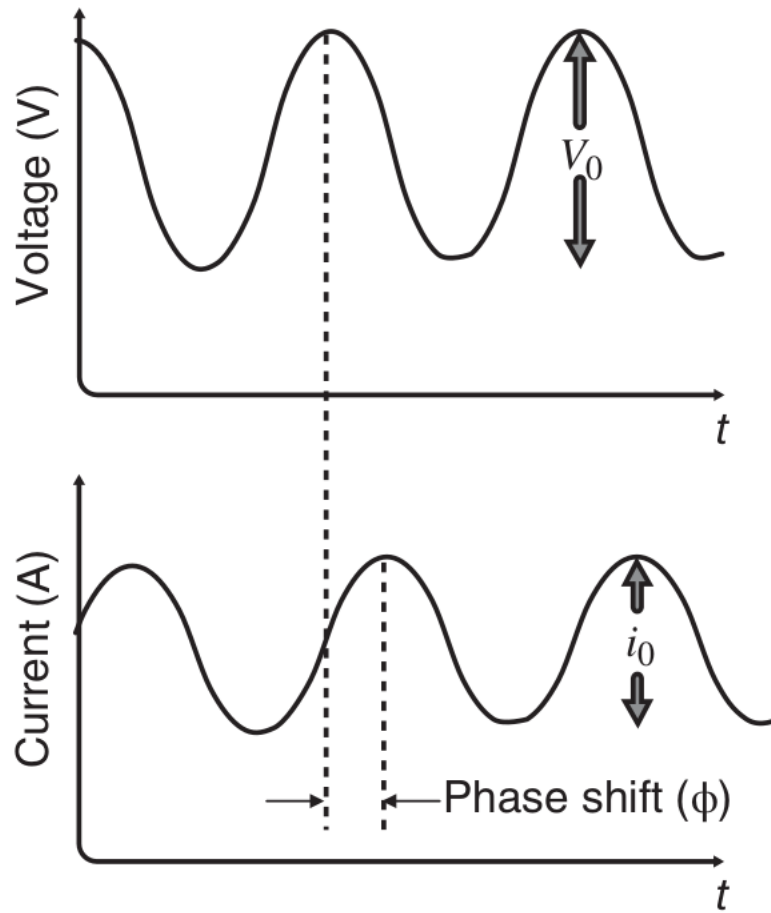f = cyclic frequency (Hz) and t = time (s).

10

Figure 2.3: Sinusoidal voltage perturbation and resulting current response

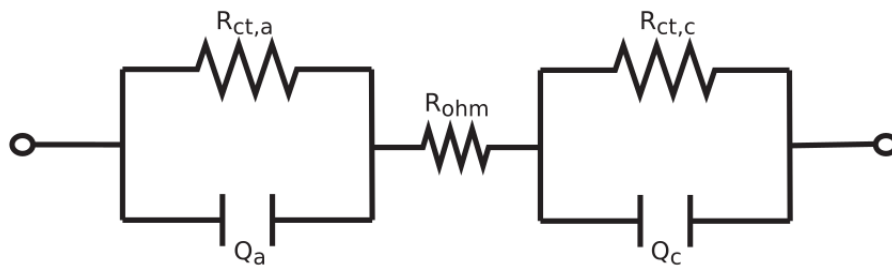
Figure 2.4: Randles circuit showing R and C elements. Here a - anode, ohm - memrane, c - cathode

After applying perturbation to the cell modelled as Fig. 2.4, resulted current will be

$$i_{\text{cell}} = i_{\text{st}} + i_{\text{p}} \sin(\omega t - \phi) \tag{2.9}$$

To obtain impedance, i_{p} and ϕ are needed to be calculated numerically.

As given in [8] multiply Eq. 2.9 with $\sin(\omega t)$

$$i_{\text{cell}}\sin(\omega t) = i_{\text{st}}\sin(\omega t) + i_{\text{p}}\sin(\omega t - \phi)\sin(\omega t) \tag{2.10}$$

integrate it from 0 to Period τ

$$\int_0^\tau i_{\text{cell}}\sin(\omega t)dt = \int_0^\tau i_{\text{st}}\sin(\omega t)dt + \int_0^\tau i_{\text{p}}\sin(\omega t - \phi)\sin(\omega t)dt \tag{2.11}$$

$$\int_0^\tau i_{\text{cell}}\sin(\omega t)dt = \int_0^\tau i_{\text{st}}\sin(\omega t)dt + i_p \int_0^\tau \sin^2(\omega t)\cos\phi dt - i_{\text{p}} \int_o^\tau \cos(\omega t)\sin(\omega t)\sin\phi dt \tag{2.12}$$

Taking 1st term on RHS of Eq. 2.12

$$\int_0^\tau i_{\text{st}}\sin(\omega t)dt = -i_{\text{st}} \left[\frac{\cos(\omega t)}{\omega} \right]_0^\tau$$

$$= \frac{i_{\text{st}}}{\omega}(1 - \cos(\omega\tau)) \tag{2.13}$$

Taking 2nd term on RHS of Eq. 2.12

$$i_{\text{p}} \int_0^\tau \sin^2(\omega t)\cos\phi dt = i_{\text{p}}\cos\phi \int_0^\tau \frac{1 - \cos(2\omega t)}{2}dt$$

$$= \frac{i_p\cos\phi}{2} \left[t - \frac{\sin 2(\omega t)}{2\omega} \right]_0^\tau$$

$$= \frac{i_p\cos\phi}{2} \left[\tau - \frac{\sin(2\omega\tau)}{2\omega} \right] \tag{2.14}$$

Taking 3rd term in Eq. 2.12

$$i_p \int_o^\tau \cos(\omega t)\sin(\omega t)\sin\phi dt = \frac{i_p\sin\phi}{2} \int_0^\tau 2\sin(\omega t)\cos(\omega t)dt$$

$$= \frac{i_p\sin\phi}{2} \int_0^\tau \sin(2\omega t)dt$$

$$= \frac{-i_p\sin\phi}{2} \left[\frac{\cos(2\omega t)}{2\omega} \right]_0^\tau$$

$$= \frac{i_p\sin\phi}{4\omega} [1 - \cos(2\omega\tau)] \tag{2.15}$$

Substituting Eq. 2.13, 2.14, 2.15 in Eq. 2.12

$$\int_0^\tau i_{\text{cell}}\sin(\omega t)dt = \frac{i_{\text{st}}}{\omega}(1 - \cos\omega\tau) + \frac{i_p\cos\phi}{2} \left(\tau - \frac{\sin(2\omega\tau)}{2\omega} \right) - \frac{i_p\sin\phi}{4\omega}(1 - \cos(2\omega\tau)) \tag{2.16}$$

Now applying the properties of sin and cos results

$$\sin(n\pi) = 0 \qquad \text{for all values of n} \tag{2.17}$$

12

$$\cos(n\pi) = -1 \qquad \text{when n is odd}$$

$$= 1 \qquad \text{when n is even} \tag{2.18}$$

Since $\omega = 2\pi f$ in our case all cos terms will become even and sin terms will vanish, so we obtain

$$\frac{i_{\text{st}}}{\omega}\left(1 - \cos(\omega\tau)\right) = 0 \tag{2.19}$$

$$\frac{i_p \sin\phi}{4\omega}\left(1 - \cos(2\omega\tau)\right) = 0 \tag{2.20}$$

and

$$\sin(\omega\tau) = 0 \tag{2.21}$$

substituting Eq. 2.19, 2.20, 2.21 in Eq. 2.16 gives

$$\int_0^\tau i_{\text{cell}}\sin(\omega t)dt = \frac{i_p(\cos\phi)\tau}{2}$$

$$i_p\cos\phi = \frac{2}{\tau}\int_0^\tau i_{\text{cell}}\sin(\omega t)dt \tag{2.22}$$

Similarly multiplying Eq. 2.9 with $\cos(\omega t)$ and integrating from 0 to period τ

integrate it from 0 to Period τ

$$\int_0^\tau i_{\text{cell}}\cos(\omega t)dt = \int_0^\tau i_{\text{st}}\cos(\omega t)dt + \int_0^\tau i_p\sin(\omega t - \phi)\cos(\omega t)dt \tag{2.23}$$

$$\int_0^\tau i_{\text{cell}}\cos(\omega t)dt = \int_0^\tau i_{\text{st}}\cos(\omega t)dt + i_p\int_0^\tau \sin(\omega t)\cos(\omega t)\cos\phi - i_p\int_o^\tau \cos^2(\omega t)\sin\phi \tag{2.24}$$

Taking 1st term on RHS of Eq. 2.24

$$\int_0^\tau i_{\text{st}}\cos(\omega t)dt = i_{\text{st}}\left[\frac{\sin(\omega t)}{\omega}\right]_0^\tau$$

$$= \frac{i_{\text{st}}\sin(\omega t)}{\omega} \tag{2.25}$$

Taking 2nd term on RHS of Eq. 2.24

$$\frac{i_p\cos\phi}{2}\int_0^\tau 2\sin(\omega t)\cos(\omega t)dt = \frac{i_p\cos\phi}{2}\int_0^\tau \sin(2\omega t)dt$$

$$= \frac{i_p\cos\phi}{2}\left[\frac{-\cos(2\omega t)}{2\omega}\right]_0^\tau$$

$$= \frac{i_p\cos\phi}{4\omega}\left[1 - \cos(2\omega\tau)\right] \tag{2.26}$$

Taking 3rd term in Eq. 2.24

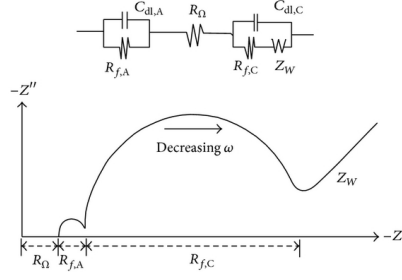$$i_p\int_o^\tau \cos^2(\omega t)\sin\phi = \frac{i_p\sin\phi}{2}\int_0^\tau (\cos(2\omega t + 1))dt$$

Figure 2.5: Nyquist plot for simple fuel cell model

$$= \frac{i_p \sin\phi}{2}\left[\frac{\sin(2\omega t)}{2\omega} + t\right]_0^\tau$$

$$= \frac{i_p \sin\phi}{4\omega}(\sin(2\omega\tau) + 2\omega\tau) \tag{2.27}$$

Substituting Eq. 2.25, 2.26, 2.27 in Eq. 2.24

$$\int_0^\tau i_{\text{cell}}\cos(\omega t)dt = \frac{i_{\text{st}}\sin(\omega\tau)}{\omega} + \frac{i_p\cos\phi}{4\omega}(1 - \cos(2\omega\tau)) - \frac{i_p\sin\phi}{4\omega}(\sin(2\omega\tau) + 2\omega\tau) \tag{2.28}$$

Now applying the properties of sin and cos results

$$\sin(n\pi) = 0 \qquad \text{for all values of n} \tag{2.29}$$

$$\cos(n\pi) = (-1) \qquad \text{when n is odd}$$

$$= 1 \qquad \text{when n is even} \tag{2.30}$$

Since $\omega = 2\pi f$ in our case all cos terms will become even and sin terms will vanish, so we obtain

$$\frac{i_p\cos\phi}{4\omega}(1 - \cos(2\omega\tau)) = 0 \tag{2.31}$$

and

$$\sin(\omega\tau) = 0 \tag{2.32}$$

substituting Eq. 2.31 and 2.32 in Eq. 2.28 gives

$$\int_0^\tau i_{\text{cell}}\cos(\omega t)dt = \frac{i_p\sin\phi}{4\omega}(0 + 2\omega\tau)$$

$$i_p\sin\phi = -\frac{2}{\tau}\int_0^\tau i_{\text{cell}}\cos(\omega t)dt \tag{2.33}$$

on solving Eq. 2.22 and 2.33, i_p and ϕ are obtained and impedance is found as follows

$$Z = \frac{V_{\text{cell}}}{i_{\text{cell}}} = \frac{V_p\exp(j\omega t)}{i_p\exp(j\omega t - j\phi)} \tag{2.34}$$

$$= \frac{V_p}{i_p}\cos\phi + j\frac{V_p}{i_p}\sin\phi \tag{2.35}$$

This is repeated for required frequency range and Nyquist plot is drawn as shown in Fig. 2.5, From

14

the graph x-axis intercepts R_Ω gives membrane resistance, R_{fa} and R_{fc} give Faradaic resistances of anode and cathode respectively. The vertical component Z_ω is warburg element and represents mass transport resistance or concentration losses.

CHAPTER 3

MY MODEL

As mentioned earlier high temperature polymer electrolyte membrane fuel cells (HTPEM) are better in managing water transport, CO tolerance and are with improved kinetics when compared to low temperature polymer electrolyte membrane fuel cells (LTPEM). Experimental work carried out by our group member [9] and [10] used to validate the model. In this data GDL is prepared using BAM carbon cloth. Catalyst slurry consisting of commercial 40% Pt/C (Arora Mathey) catalyst is dried on GDL and dried to form a catalyst layer with loading of 1 mg/cm^2 at anode and cathode.

3.1   Model Framework

3.1.1   Charge Transfer

The general form of Butler-Volmer equation is used for modelling of HOR and ORR and given as

$$i = i_0 \left[\exp\left(\frac{\alpha_a F \eta_a}{RT} \right) - \exp\left(\frac{-\alpha_c F \eta_a}{RT} \right) \right] \tag{3.1}$$

Where, i_0 = exchange current density and expressed as a function of partial pressures or coverages of reactant species with arbitrary order dependency,
F = Faradays constant (C/mol),
η_a = overpotential at anode (V),
η_c = overpotential at cathode (V),
α_a and α_c are charge transfer coefficinets of HOR and ORR respectively.
    Eq. 3.1 is valid only for single electron transfer reactions.

3.1.2   Hydrogen oxiation kinetics

Oxidation of Hydrogen follows below reaction mechanisms in presence of CO
Tafel reaction

$$H_2 + 2* \leftrightarrow H(*) + H(*) \tag{3.2}$$

Volmer reaction

$$H(*) \leftrightarrow H^+ + e^- + * \tag{3.3}$$

Table 3.1: Rate equation models for hydrogen oxidation reaction

Model	Current density(i_a)	Exchange current density(i_{oa})
Volmer-Tafel	$i_{oa}[exp(\beta_a f\eta_a) - exp(-\beta_c f\eta_a)]$	$i_a^* \dfrac{(K_{H_2}p_{H_2})^{(1-\beta_a)/2}}{1+K_{CO}p_{CO}+(K_{H_2}p_{H_2})^{1/2}}$
Tafel-Volmer	$i_{oa}\dfrac{[1-exp(-2f\eta_a)]}{[1+K_{CO}p_{CO}+(K_{H_2}p_{H_2})^{1/2}exp(-f\eta_a)^2]}$	$i_a^*\bar{p}_{H_2}$
Heyrovsky-Volmer	$i_{oa}\dfrac{[exp(\beta_a f\eta_a)-exp(-(1+\beta_c)f\eta_a)]}{[1+K_{CO}p_{CO}+(K_{H_2}p_{H_2})^{1/2}exp(-f\eta_a)]}$	$i_a^*\bar{p}_{H_2}^{(1-\beta_a)/2}$
Volmer-Heyrovsky	$i_{oa}\dfrac{[[exp((1+\beta_a)f\eta_a)-exp(-\beta_c f\eta_a)]]}{[1+K_{CO}p_{CO}+(K_{H_2}p_{H_2})^{1/2}exp(f\eta_a)]}$	$i_a^*\bar{p}_{H_2}^{(\beta_c)/2}$
Tafel-Heyrovsky	$i_{oa}\dfrac{[[1-exp(2f\eta_a)]]}{[1+K_{CO}p_{CO}+(K_{H_2}p_{H_2})^{1/2}exp(f\eta_a)^2]}$	$i_a^*\bar{p}_{H_2}$
Heyrovsky-Tafel	$i_{oa}[exp(\beta_a f\eta_a) - exp(-\beta_c f\eta_a)]$	$i_a^*\bar{p}_{H_2}^{(1-\beta_a)}\dfrac{(K_{H_2}p_{H_2})^{(\beta_a/2)}}{1+(K_{H_2}p_{H_2})^{1/2}+K_{CO}p_{CO}}$

Heyrovsky reaction

$$H_2 + * \leftrightarrow H^+ + e^- + H(*) \tag{3.4}$$

Adsorption of CO

$$CO + * \leftrightarrow CO(*) \tag{3.5}$$

Here * denotes vacant adsorption site on catalyst layer (Pt). Rate expressions are derived by assuming any one of the above mentioned reactions as rate determining step and other reactions to be in equillibrium. In this way total six formulations are formed as shown in table 3.1.

In above mentioned models only Volmer-Tafel and Heyrovsky-Tafel are giving Butler-Volmer type kinetics for current density (A/cm^2). In given models i_{oa} is volumetric exchange current density at anode A/cm^3, f = F/RT, β_a and β_c are symmetric factors for anode and cathode respectively, p_i is the partial pressure of ith species, $\bar{p}$ is the normalized pressure, K_k is the equillibrium constant and i_a^* is the lumped parameter of all the constants.

3.1.3 Oxygen reduction kinetics

The adsorption of O$_2$ follows dissociative adsorption above 150 K. Reaction mechanism is as follows

$$O_2 + 2* \leftrightarrow 2O(*) \tag{3.6}$$

$$O(*) + H^+ + e^- \leftrightarrow OH(*) \tag{3.7}$$

$$OH(*) + H^+ + e^- \leftrightarrow H_2O(*) \tag{3.8}$$

$$H_2O(*) \leftrightarrow H_2O + * \tag{3.9}$$

It results in Butler-Volmer type kinetics for current density only if Eq. 3.7 and 3.8 are choosen as rds. By choosing Eq. 3.7 as rds the resulting current density is in the form

$$i = i_{oc}exp[(1 + \beta_a)f\eta_c] - exp(-\beta_c f\eta_c) \tag{3.10}$$

and exchange current density is in the form

$$i_{oc} = i_c^* \frac{(K_{H_2O}p_{H_2O})^{\beta_c/2}(K_{O_2}p_{O_2})^{(2-\beta_c)/4}}{1 + (K_{O_2}p_{O_2})^{1/2} + K_{H_2O}p_{H_2O}[1 + exp(\Delta G^*/RT)]} \tag{3.11}$$

Where, ΔG^* is the change in free energy in J/mol, i_c^* is the lumped parameter similar to i_a^*

17

From above equation it is evident that exchange current density at cathode is dependent on partial pressure of H_2O.

3.1.4 Equillibrium constant calculation

The equillibrium constants K_i are calculated based on the adsorption of reactant species and desorption of product species [2]. Sticking coefficient is a new constant introduced to represent the adsorption of gas species on Pt surface and can be converted to rate expression as follows.

$$r_{i,a} = \gamma_i \sqrt{\frac{RT}{2\pi M_i}} \frac{p_i}{RT} \theta_{Pt}^n \tag{3.12}$$

Where, γ_i is sticking coefficient of the ith species,
M_i is the molecular weight in (kg/mol),
θ_{Pt} is the fraction of vacant sites on the catalyst surface, and
n is the required number of sites.

$$r_{i,d} = k_d exp(\frac{-E_d}{RT})\theta_i^n \Gamma^n \tag{3.13}$$

Where, Γ is the total site density in (mol/m^2),
θ_i is the fraction of coverage on Pt surface by species.

So final form of equation for equillibrium constant is

$$K_i = \frac{\theta_i^n}{p_i \theta_{pt}^n} = \frac{\gamma_i exp(-\frac{E_d}{RT})}{\Gamma^n k_d \sqrt{2\pi M_k RT}} \tag{3.14}$$

Where, E_d is the desorption energy for associative desorption of H_2 on Pt surface and is reported to be 21 kJ/mol [5].

3.2 Numerical model

3.2.1 Species transport

The experiments that are considered here for the purpose of model validation is done at high flow rates and species consumption is low (3% H_2 and 9% O_2) so concentration of reactant species do not vary along the flow channel and resolving is done only through the thickness of MEA. The species transport along the MEA is given by

$$\frac{\partial(\epsilon\rho Y_i)}{\partial t} = \frac{-\partial j_k}{\partial y} + \dot{s}_{i,e} M_i \tag{3.15}$$

Where, Y_k is the mass fraction of species i,
ϵ is the porosity,
ρ is the density (kg/m^3),
j_k is the mass flux of the species in kg m^2 s^{-1},
y is independent coordinate,
t is time in s.
$\dot{s}_{i,e}$ is the molar production of species i due to electrochemical reaction and is given by

$$\dot{s}_{i,e} = \pm \frac{i}{n_e F} \tag{3.16}$$

Where, n_e is number of electrons transferred per mole of species.

Dusty gas model (DGM) is utilized to calculate the flux (j_i)

$$\frac{j_i}{M_i} = \Sigma_{i=1}^{N_g} D_{il}^{DGM} \bigtriangledown [X_i] - \left[\Sigma_{k=i}^{N_g} D_{il}^{DGM} \frac{X_i}{D_{l,Kn}^e}\right] \frac{B_g}{\mu} \bigtriangledown p \tag{3.17}$$

Here, $[X_i]$ is the concentration of ith species in (mol/m^{-3}),

B_g is the permeability in m^2,

X_i is the mole fraction of species i,

μ is the viscosity in kg m^{-1}s^{-1},

p is the total pressure in Pa.

D_{il}^{DGM} in turn given by

$$D_{il}^{DGM} = H^{-1} \tag{3.18}$$

H matrix elements are given by

$$h_{kl} = \left[\frac{1}{D_{i,Kn}^e} + \Sigma_{j \neq k} \frac{X_j}{D_{ij}^e} \delta_{il} + (\delta_{il} - 1) \frac{X_i}{D_{il}^e}\right] \tag{3.19}$$

Where, $D_{i,Kn}^e$ is effective Knudsen diffusion coefficient and is given by

$$D_{i,Kn}^e = \frac{\epsilon}{\tau} \frac{d_p}{3} \sqrt{\frac{8RT}{\pi M_i}} \tag{3.20}$$

Where, d_p is the pore diameter in (μm).

Here ideal gas equation is used to calculate the total pressure

$$p\bar{M} = \rho RT \tag{3.21}$$

Here, $\bar{M}$ is the average molecular weight in (kg/mol).

3.2.2 Charge trasport

The charge transport equations are given below which solve for current and potential in catalyst layer since we are assuming GDL is with high electrical conductivity. So electrical potential is uniform throughout the GDL. The equations are

Cathode electric potential:

$$C_{dl} \frac{\partial(\varphi_{e,c} - \varphi_{i,c})}{\partial t} = \frac{\partial}{\partial y}\left(\sigma_e^e \frac{\partial \varphi_{e,c}}{\partial y}\right) - i_c \tag{3.22}$$

Cathode ionic potential:

$$C_{dl} \frac{\partial(\varphi_{i,c} - \varphi_{e,c})}{\partial t} = \frac{\partial}{\partial y}\left(\sigma_i^e \frac{\partial \varphi_{i,c}}{\partial y}\right) + i_c \tag{3.23}$$

Anode electric potential:

$$C_{dl} \frac{\partial(\varphi_{e,a} - \varphi_{i,a})}{\partial t} = \frac{\partial}{\partial y}\left(\sigma_e^e \frac{\partial \varphi_{e,a}}{\partial y}\right) - i_a \tag{3.24}$$

Anode ionic potential:

$$C_{dl} \frac{\partial(\varphi_{i,a} - \varphi_{e,a})}{\partial t} = \frac{\partial}{\partial y}\left(\sigma_i^e \frac{\partial \varphi_{i,a}}{\partial y}\right) + i_a \tag{3.25}$$

Here, $\varphi_{e,a}$ = electric potential at anode,

$\varphi_{i,a}$ = ionic potential at anode,
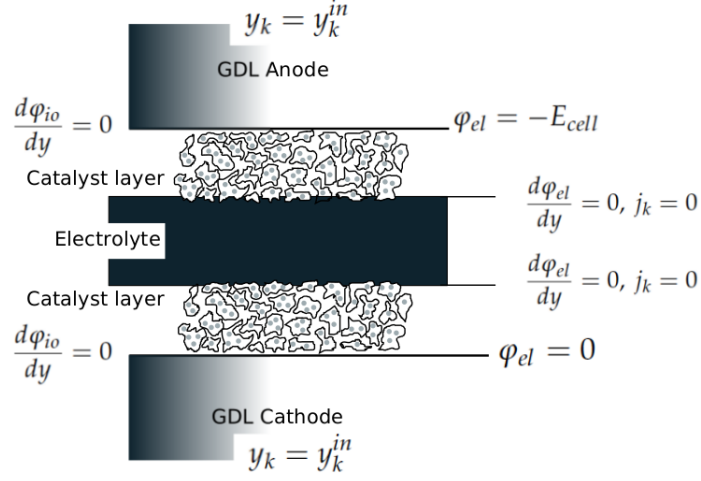
$\varphi_{e,c}$ = electric potential at cathode,

Figure 3.1: Boundary conditions

$\varphi_{i,c}$ = ionic potential at cathode,

C_{dl} = double layer capacitance between ions and electrons,

σ_i^e, σ_e^e are the effective ionic and electric conductivities of catalyst layer.

Here C_{dl} is taken to be constant and does not affect the solution of above equations.

The activation overpotential in the Eq. 3.1 is given by the equation in terms of ionic and electric potentials.

At cathode:

$$\eta_c = \varphi_{e,c} - \varphi_{i,c} - E_{rev} \tag{3.26}$$

At anode:

$$\eta_a = \varphi_{e,a} - \varphi_{i,a} \tag{3.27}$$

Where, E_{rev} is the reversible potential given by Nernst equation (Eq. 2.1).

3.3 Boundary conditions

Boundary conditions are needed to solve the Eq. 3.22, 3.23, 3.24 and 3.25. Conditions are specified at electrode-flow channel interface and electrode-electrolyte interface [9]. Species compostion acts as boundary condition at the channel and electrode interface [10]. Similarly zero flux boundary condition is imposed at electrode-electrolyte interface since electrolyte does not allow gas species to transport through it.

Electric potential is set as operating voltage at anode CL-GDL interface and at cathode CL-GDL interface it is set to zero. Ions are confined to the catalyst layer and do not pass through the GDL on either side its flux is set to zero at the interface of GDL-CL. Electrolyte conducts solely ions so at the interface of electrolyte and catalyst layer electric potential flux is set as zero. All boundary conditions are shown schematically in Fig. 3.1

CHAPTER 4

RESULTS AND DISCUSSION

After forming the model it is needed to be validated by comparing with relevant experimental data from the literature. Model needs few specified parameters to be tuned in order to fit the data. Our model is validated for multiple cases [10, 1, 3]. We have taken one of our group members data to analyse the validity of six different HOR models [10]. The dynamics of CO poisoning i.e., the response of normalized current density has been obtained by the model and is fitted for the data from ref. [1]. The data for overpotentials of anode and cathode have been taken taken from [3] and complementary trends were obtained from the model.

In the process of validation we have tuned mainly exchange current density $i*$ and symmetric factor β. The order dependency of the exchange current density on the concentration of reactants and products is a result of derivation of Butler-Volmer equation. It is evident that order depends on symmetric factor β. The equillibrium constants appeared in the model are calculated from adsorption-desorption equillibrium of the reactions [10]. The data choosen from our own group is validated as follows. The experimental details are given in [10].

Different HOR models are compared for the data using same set of tuning parameters i.e., exchange current density is shown in Fig. 4.1. From figure we can observe that all the models are producing the same results expect Heyrovsky-Tafel model which is predicting somewhat lower performance. Indeed, we can fit experimental data using any of these models by slightly adjusting fit parameters. For all the results obtained Volmer-Tafel type model is used since most of the literature refers to it.

The experimental data of one of our group members shown in Fig. 4.1 is carried out at 140, 150 and 160 ^{o}C respectively [10]. As it can be seen from Fig. 4.1 a very good agreement is obtained between model predictions and experimental results. To proceed further our main fitting parameters exchange current densities i_a^* and i_c^* have to be expressed as function of temperature. We have used Arrhenius equation to relate exchange current density and temperature and is given by

$$i^* = i' exp(E'/RT) \tag{4.1}$$

As mentioned before polarization curves are obtained using Volmer-Tafel model and is shown in Fig. 4.2. In this case pure H_2 at anode side and air at cathode side are sent and the physical properties of MEA
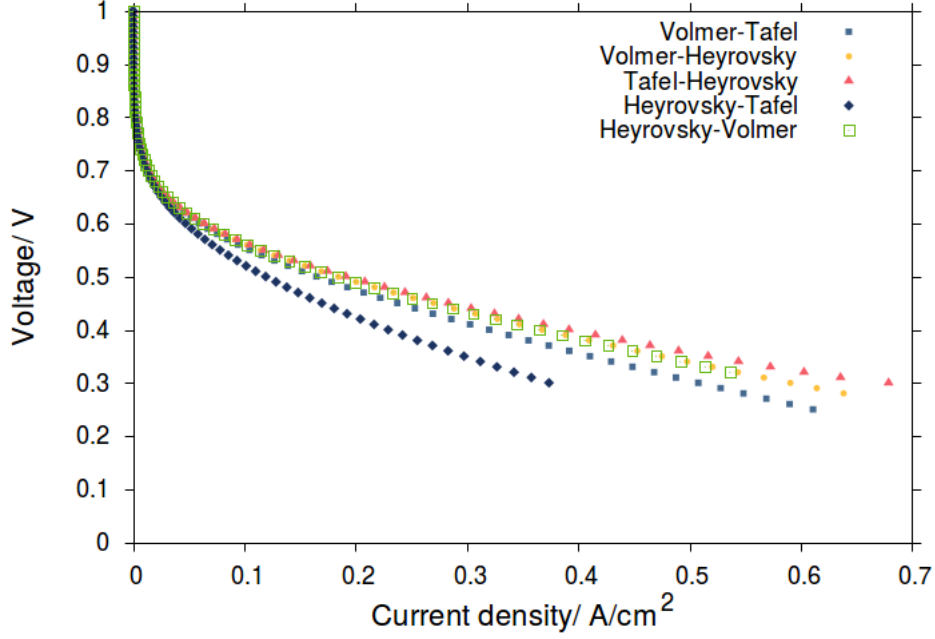
Figure 4.1: Comparison of different HOR models

Table 4.1: Table showing physical properties of MEA

Parameter	GDL Anode	CL Anode	GDL Cathode	CL Cathode	Electrolyte
Thickness(μm)	330	50	330	50	55
Porosity	0.4	0.25	0.4	0.25	-
Tortuosity	2.5	2.5	3.5	2.5	-
Pore diameter(μm)	1.0	1.0	1.0	1.0	-
Ionic volume fraction	-	0.3	-	0.3	1.0
Electrical conductivity (S/m)	250	250	250	250	0
Ionic conductivity					
σ(S/m)	0	7×10^6	0	7×10^6	7×10^6
E(J/mol)	0	2.5×10^6	0	2.5×10^6	2.5×10^6

are given in table 4.1. By further introducing one more fitting parameter pore diameter which was 1 μm in Fig. 4.2 is decreased to 0.01 μm. The modified iV curve is shown in Fig. 4.3. It is observed that model predictions and experimental data is well matched. However when we operate with oxygen at cathode, needed to compromise at 160 ^{o}C for air and pure O_2 in obtaining the best fit as shown in Fig. 4.2. The current density calculated is the ionic flux through the memrane which is equal to the integrated current through out the catalyst layer. Initially experimental data is fitted at 160 ^{o}C and 140 ^{o}C. Since we are sending pure hydrogen at anode side exchange current density and symmetric factor on anode side are kept constant at 500(A/cm^3) and 0.7 respectively. Fitting is carried out by adjusting fitting parameters solely on cathode side. The obtained parameters at 160 ^{o}C and 140 ^{o}C are substituted in Arrhenius equation to get the same at 150 ^{o}C the values of which are shown in table 4.2. Arrhenius constants such as i' and E' are used to calculated exchange current density at 150 ^{o}C are shown in table 4.3.

To judge the uniqueness of the parameters it is not sufficient to fit solely polarization curves. It should reproduce the polarization curves and activation losses with the same set of parameters. Data reported by Kaserer et al. is simulated here to ascertain the validity of fitted parameters [3]. In this experimetal work

22

Table 4.2: Fitting parameters for Fig. 4.2 and 4.3

Temperature	Parameter	HOR	ORR
160^oC	$i^*(\mathrm{A/cm^3})$	500	1.8×10^{-3}
	β	0.7	0.3
150^oC	$i^*(\mathrm{A/cm^3})$	500	7.8×10^{-4}
	β	0.7	0.3
140^oC	$i^*(\mathrm{A/cm^3})$	500	3.3×10^{-4}
	β	0.7	0.3

Table 4.3: Arrhenius constants

Parameter	ORR
i'$(\mathrm{A/cm^3})$	2.9×10^{12}
E'(kJ/mol)	126.05
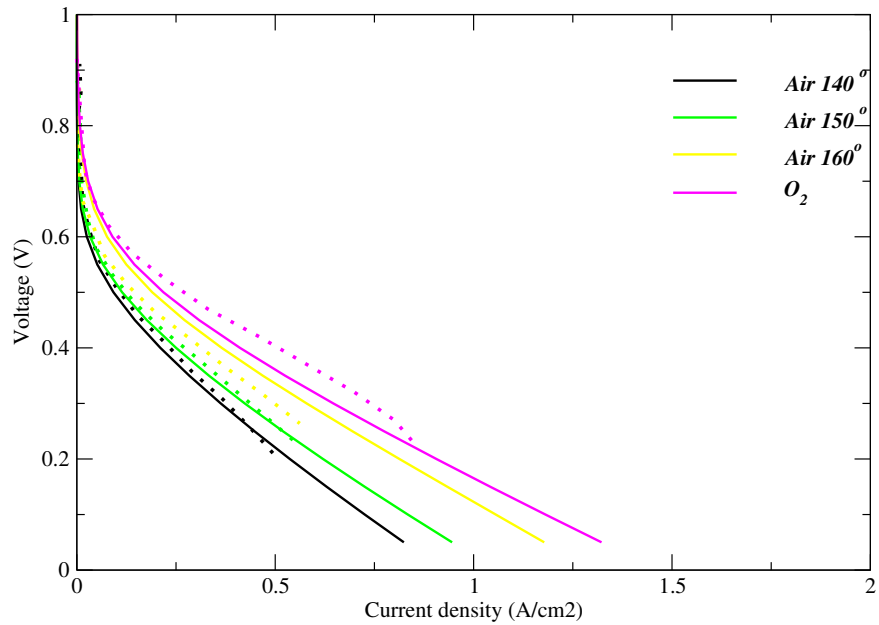
Figure 4.2: iV fit of Anushree et al [10]
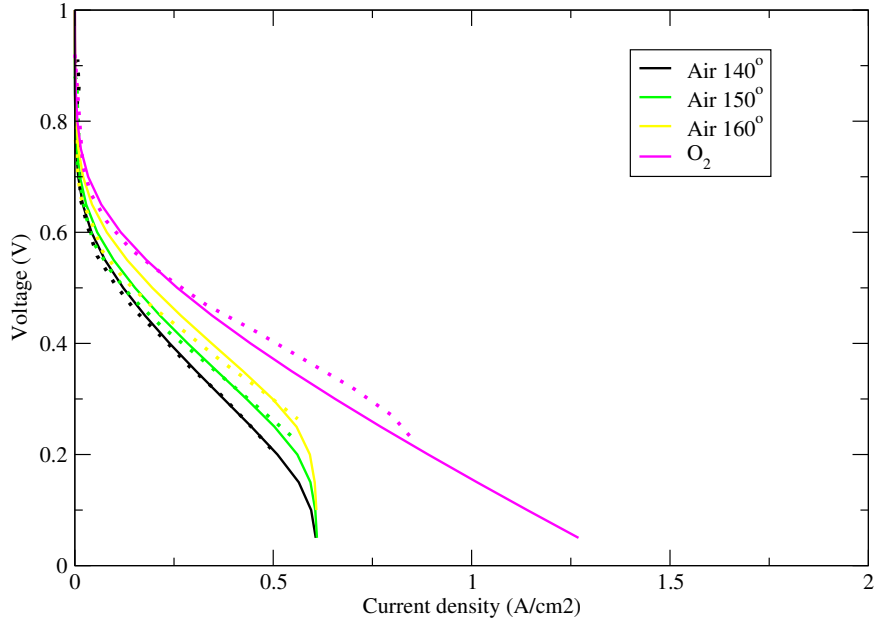
Figure 4.3: Modified iV fit of Anushree et al [10]

Table 4.4: Parameters for Kaserer et al.

Parameter	HOR	ORR
i*	20	0.025
β	0.7	0.4

pure hydrogen is sent on anode side and O_2/N_2 ratio of 1/4 is sent on cathode side. All the experimetal work is done at the temperature of 160^oC.

Aforementioned parameters i* and β are adjusted to fit the polarization curves and the same set of parameters produced activation overpotential predictions at anode as well as cathode which agree very well with the experimental data as shown in Fig. 4.4, 4.5 and 4.6. The parameters are shown in table 4.4.

In Fig. 4.5 anode overpotential is calculated using Eq. 3.27 and the product of current and resistance (current collectors and cables) is substracted from it [3]. Cathode overpotential is calculated directly using Eq. 3.26 and is shown in Fig. 4.6.

Apart from these a transient simulation is performed to obtain the dynamic response of CO poisoning [1]. In this experiment DC polarization measurement is carried out at 150^oC by sending pure hydrogen at anode and air at cathode. Experimentally determined iV curves are simulated and showed a good agreement as shown in Fig. 4.7. The main objective of the experiment is to study the influence of CO in the reactant on the performance of the fuel cell. The trasient response is carried out at the voltage of 0.6V. Initially the cell is run with pure H_2 for 4 min, then the pulse input of CO with 1.31 mole %. The current density obtained with presence of CO is normalised by dividing it with the current density obtained with pure H_2. The presence of CO caused the current density to fall to nearly 75% of that with pure H_2 as shown in Fig. 4.8. Cell is run for 17 min with CO and then switched to pure H_2. It has taken around 20 min to stablilize and attained the original current density. A well matching model response plot is shown in Fig. 4.8.

We tried to model the electrochemical impedance spectroscopy results of our group member which needs
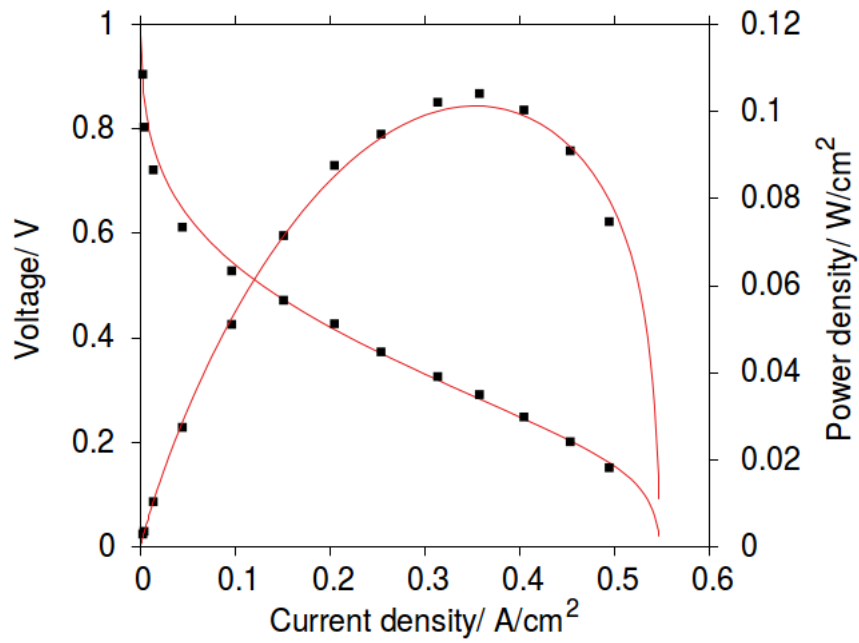
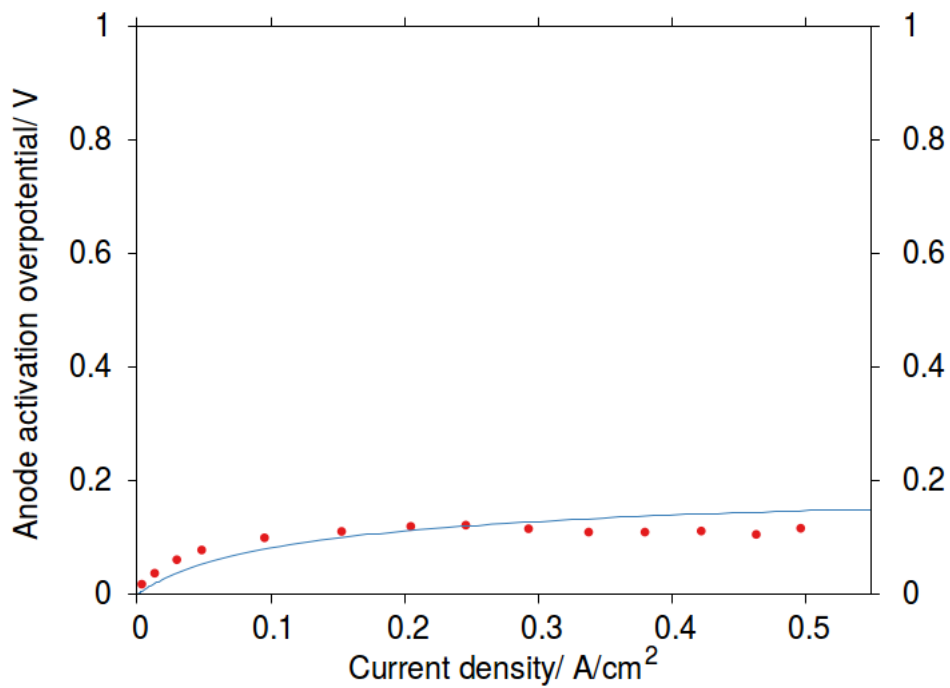Figure 4.4: iV fitting of Kaserer et al.

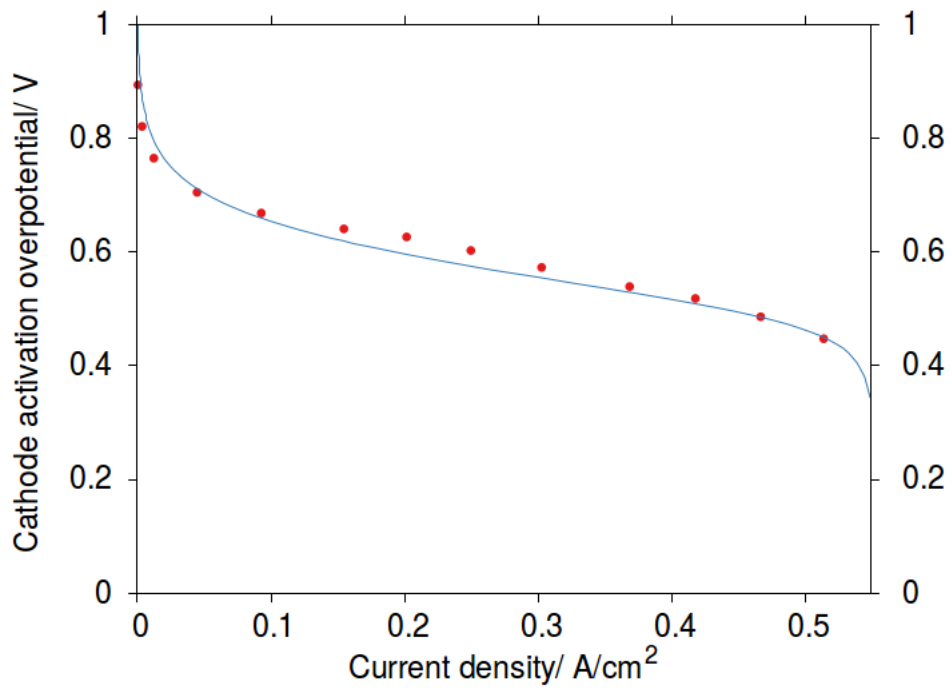Figure 4.5: Prediction of anode overpotential of Kaserer et al.

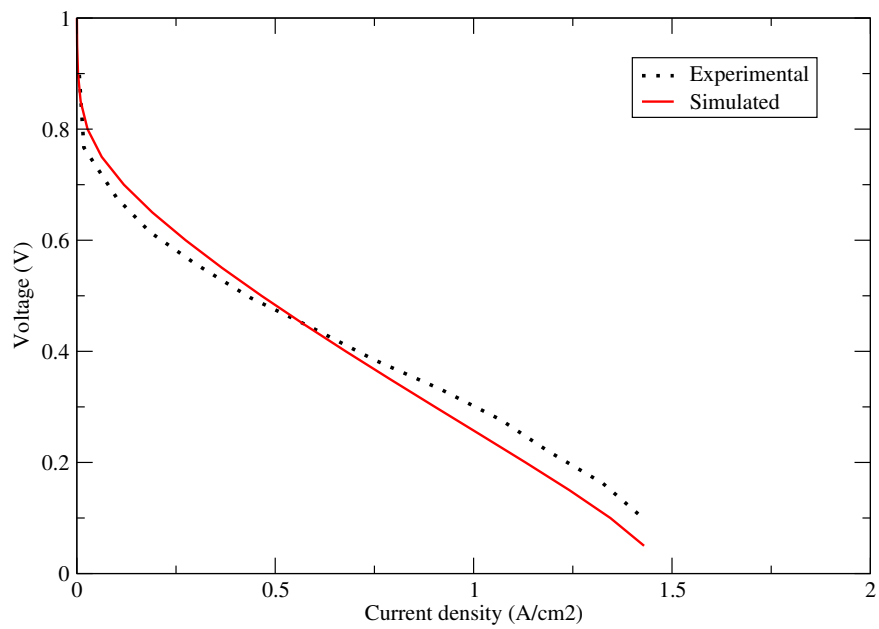Figure 4.6: Prediction of cathode overpotential of Kaserer et al.

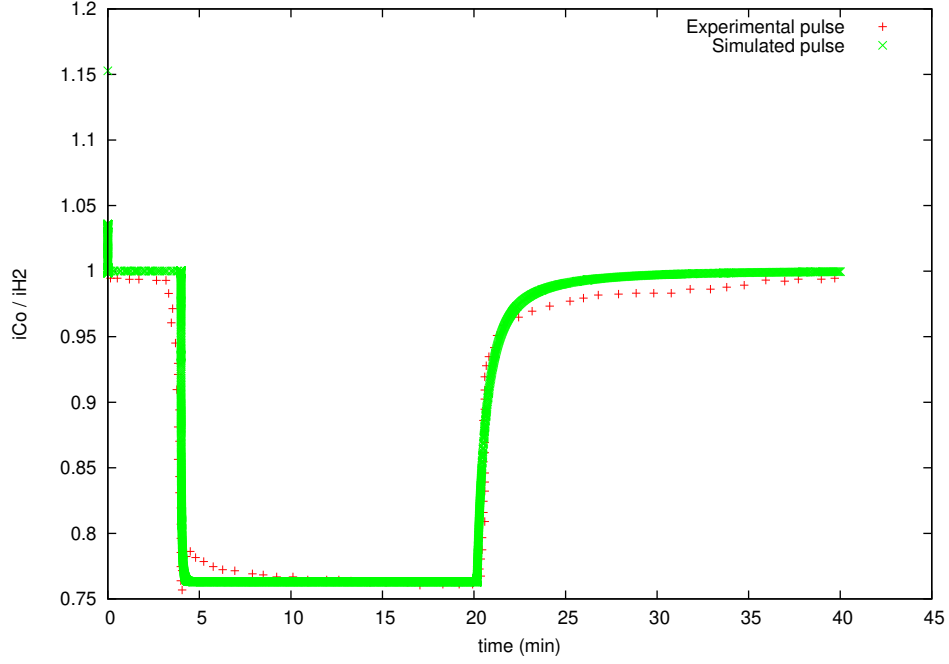Figure 4.7: iV fit of Bergmann et al.

Figure 4.8: Normalized current density simulation of Bergmann et al.

Table 4.5: Parameters for EC model

Parameter	Anode	Cathode
Charge transfer resistance(Ω/cm^2)	0.12	0.5
Double layer capacitance (F/cm^2)	0.16	0.3

a equivalent circuit model. The EC model of the type shown in Fig. 2.4 is assumed and parameters of the same are obtained. Experimental work was done at the temperature of $160^{o}C$ and the impedance data is taken at the same for the validation. The parameters obtained as required in the EC model. The membrane resistance is obtained to be 0.142 (Ω/cm^2). The remaining parameters at anode and cathode are presented in table 4.5. We could not complete the implementation of a physically based impedance model based on the derivation given in Ch.2. This needs to be taken as the future work.
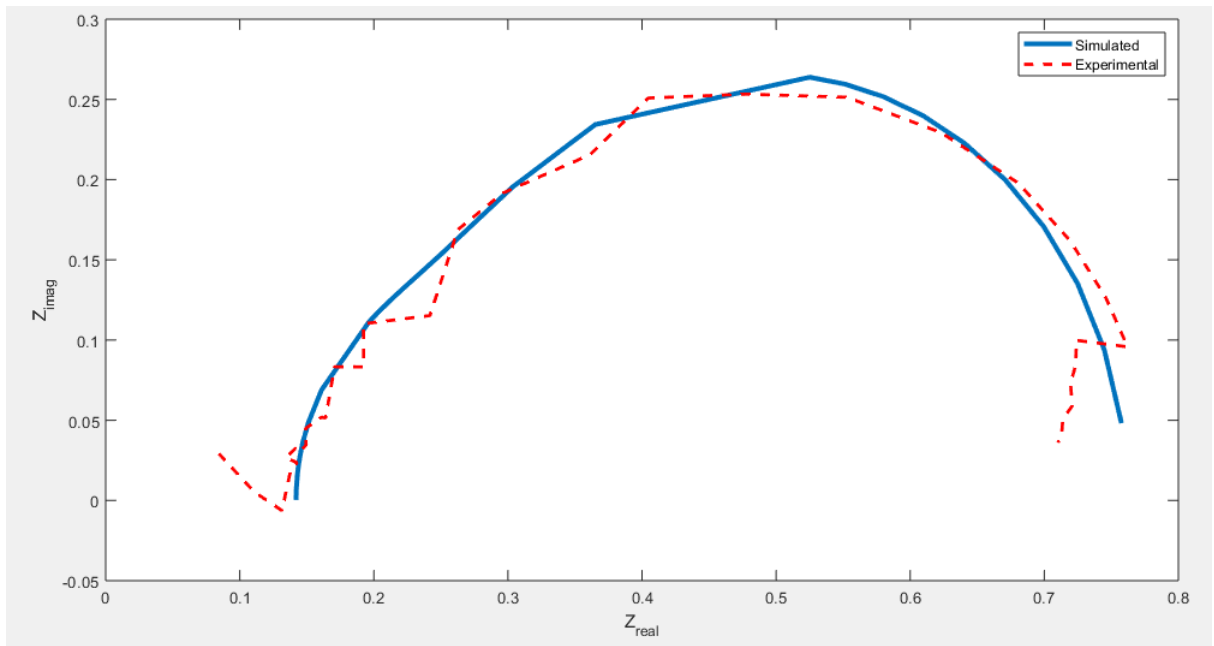
Figure 4.9: Impedance fitting through EC model

CHAPTER 5

CONCLUSIONS

Our numerical model for a HTPEM fuel cell resolves cell along the thickness of MEA. Different HOR and ORR models are presented and it is seen that same experimental data can be reproduced with all the models by adjusting fit parameters i.e., exchange current density and symmetric factor. Whereas ORR is found to be sensitive with respect to different models. Non-Butler-Volmer kinetics failed to reproduce the experimental data. It is seen that model fits the polarization data obtained experimentally and obtained overpotential data with the same fitting parameters. We can observe that ORR kinetics are very sluggish due to the presence of other gases like nitrogen, hence sensitive to tuning parameters. So efforts should be toward the enhancement of the ORR kinetics.

We can extend our model to predict the electrochemical impedance of fuel cell to get better insight of interior processes. First steady state of the system should be ensured, sinusoidal perturbation in voltage to be given with small amplitude in order to ensure linerity in the system. By solving Butler-Volmer equations in the model current response is obtained with same frequency of that voltage and with different amplitude and with some phase shift. Application of Fourier trasform produces the impedance. It is repeated in required range of frequencies and finally impedance spectra is obtained.

REFERENCES

[1] A. Bergmann, D. Gerteisen, and T. Kurz. Modelling of co poisoning and its dynamics in htpem fuel cells. *Fuel Cells*, 10(2):278–287, 2010.

[2] V. Janardhanan. A detailed approach to model transport, heterogeneous chemistry, and electrochemistry in solid-oxide fuel cells. 2007.

[3] S. Kaserer, C. Rakousky, J. Melke, and C. Roth. Design of a reference electrode for high-temperature pem fuel cells. *Journal of Applied Electrochemistry*, 43(11):1069–1078, 2013.

[4] Q. Li, J. O. Jensen, R. F. Savinell, and N. J. Bjerrum. High temperature proton exchange membranes based on polybenzimidazoles for fuel cells. *Progress in polymer science*, 34(5):449–477, 2009.

[5] J. Ludwig, D. G. Vlachos, A. C. Van Duin, and W. A. Goddard. Dynamics of the dissociation of hydrogen on stepped platinum surfaces using the reaxff reactive force field. *The Journal of Physical Chemistry B*, 110(9):4274–4282, 2006.

[6] R. O'hayre, S.-W. Cha, F. B. Prinz, and W. Colella. *Fuel cell fundamentals*. John Wiley & Sons, 2016.

[7] B. Prasad and V. M. Janardhanan. Modeling sulfur poisoning of ni-based anodes in solid oxide fuel cells. *Journal of The Electrochemical Society*, 161(3):F208–F213, 2014.

[8] Y. Shi, N. Cai, C. Li, C. Bao, E. Croiset, J. Qian, Q. Hu, and S. Wang. A general approach for electrochemical impedance spectroscopy simulation using transient mechanistic sofc model. *Ecs Transactions*, 7(1):1889–1899, 2007.

[9] A. Unnikrishnan, N. Rajalakshmi, and V. M. Janardhanan. Mechanistic modeling of electrochemical charge transfer in ht-pem fuel cells. *Electrochimica Acta*, 261:436–444, 2018.

[10] A. Unnikrishnan, N. Rajalakshmi, and V. M. Janardhanan. Kinetics of electrochemical charge transfer in ht-pem fuel cells. *Electrochimica Acta*, 293:128–140, 2019.

[11] X.-Z. R. Yuan, C. Song, H. Wang, and J. Zhang. *Electrochemical impedance spectroscopy in PEM fuel cells: fundamentals and applications*. Springer Science & Business Media, 2009.